

A FAST SPREADSHEET MODEL FOR THE YIELD STRENGTH OF SUPERALLOYS

T.A.Parthasarathy*, S.I.Rao*, D.M.Dimiduk,
Air Force Research Laboratory, AFRL/MLLM
Materials and Manufacturing Directorate
Wright-Patterson AFB OH 45433-7817

Keywords: Yield Strength, Superalloys, Model, Spreadsheet **Alloys:** Nimonic105, IN100, René88, Alloy ME3

Abstract

A methodology to rapidly evaluate the yield strength of superalloys using a fast spreadsheet model was explored. The results from a physics-based discrete dislocation simulation model were fit to polynomials. These were used along with appropriate heuristic logic, to develop a spreadsheet that can predict the yield strength from the composition, and microstructural parameters of an alloy. The model was compared with data available for a series of superalloys and found to have good correspondence.

1.0 Introduction

The nickel-based superalloys are a metallurgical marvel and have benefited from several decades of evolutionary changes. It is generally agreed by metallurgists that even in this class of the most evolved and complex alloys, the mechanical behavior is dictated almost entirely by the microstructure and chemistry of the phases. However it is also generally agreed that the ability to predict mechanical behavior poses great difficulties even when the microstructure and chemistry are well characterized in a given alloy. Of the various mechanical properties of design interest, the yield strength is likely the easiest to predict. There have been published works in which semi-empirical models were built using data from well-designed experiments with reasonable success. (see for example, Schirra¹) However for alloy design, and for studying effects of a wider range of variables, physics-based models are desired. The present work is an attempt at such a model. We begin with a brief description of the status of physics-based models, to bring out the novelty of the present work.

Decades of metallurgical research have shown that the yield behavior of alloys is due to the passage of dislocations through the microstructure, and their interactions with internal interfaces including grain boundaries. Based on simple line tension approximations for dislocations, analytical models have been developed for predicting yield strength of superalloys, for example see Ref. ²⁻⁶ These models have limited range of predictive capability since they consider mechanistic processes taken one at a time and then assume additivity rules that are ad-hoc. Thus these models might predict reasonably well the effect of a given variable (when other variables are held constant) but their predictions when more than one variable is changed simultaneously are suspect. For example, these models consider either cutting of precipitates or bowing between precipitates, but they do not address situations where both mechanisms are operative in different regions at the same time.^{2,5,6} In addition to such deficiencies, these models do not consider microstructural variability.

Simulation methods allow the possibility of overcoming some of the deficiencies of analytical models. In a recent work, we have developed a numerical model (the details of which are published elsewhere⁷) that considers the actual microstructure of a superalloy and uses accurate descriptions of dislocation behavior to predict the critical resolved shear stress for a given microstructure. This numerical model captures the physics of the problem accurately (for cutting via single APB-coupled dislocation pairs and bowing-assisted cutting), but is computationally expensive. In this work, we present an approach that uses the numerical discrete dislocation (DD) model to build a fast spreadsheet model that may be of industrial use.

The paper is organized as follows. We start with a description of the microstructure as represented in the model, and a brief overview of the approach used to derive the spreadsheet model. We then present elements of this derivation, which include the numerical DD model. Next the results of a parametric study conducted using the physics-based numerical model is presented. The predicted dependence of the yield strength of superalloys on various microstructural parameters is shown. Finally the derivation of the spreadsheet model from these parametric studies is presented; the predictions of the spreadsheet model are shown compared with experimental data.

2.0 Superalloy Microstructure Considered by the Model

The focus of this work has been on alloys for turbine disks. The superalloys used for disk applications are typically fine-grained polycrystalline materials with each grain having a fine distribution of coherent precipitates. A schematic sketch of this microstructure is shown in Figure 1. Depending on the heat treatment, the precipitates will comprise of a mixture of primary, secondary and tertiary types. The primary γ' is typically between grains of $(\gamma+\gamma')$, while the secondary and tertiary are precipitates

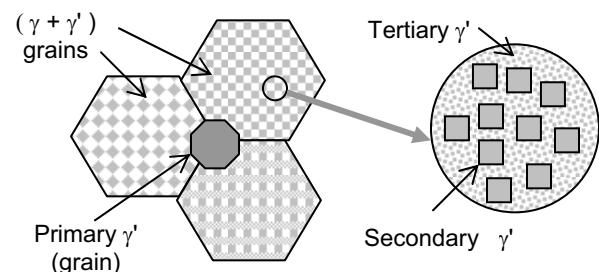


Figure 1 : Schematic sketch of the superalloy microstructure considered by the model.

*-UES, Inc.Dayton,OH, under USAF Contract #-F33615-01-C-5214

within the ($\gamma+\gamma'$) grains, with the secondary being larger and higher in volume fraction. Polycrystalline disk superalloys could be either supersolvus treated alloys or subsolvus treated alloys. The supersolvus treated alloys have little or no large primary γ' but their grain size is typically over 20 microns. The secondary γ' is typically of the order of 0.2 micron, while the tertiary γ' is of the order of 0.02 micron. On the other hand, the subsolvus treated alloys have typically very fine grains (<5 microns), but do have primary γ' grains that are of the order of a few microns in size.

The model derived in this work assumes the following microstructural characteristics of superalloys. The superalloy can be a single crystal or polycrystal. The critical resolved shear stress of single crystals is directly computed. For polycrystals, an average grain size is used. The polycrystals may contain two different types of grains, entirely γ' grains and ($\gamma+\gamma'$) grains, where γ refers to the Ni-based solid solution with FCC structure (termed 'matrix' in this work) and γ' refers to the Ni₃Al-based intermetallic phase (termed as 'precipitate' or γ' in this work). The γ' grains are referred to as primary γ' , while the γ' in the ($\gamma+\gamma'$) grains are further classified into secondary and tertiary populations. In this work, both the secondary and tertiary γ' precipitates are taken to be cuboidal in shape with a uniform size, but randomly located in space. The secondary γ' is typically 5 to 10 times larger than the tertiary γ' which are distributed uniformly in the matrix regions between the secondary γ' precipitates. In the literature, one finds that the volume fractions of the three γ' populations are given relative to the entire material. The simulations of ($\gamma+\gamma'$) grains were conducted for volume fractions defined with respect to this grain. In comparing literature data, care was taken to make the appropriate conversions.

3.0 Fast Spreadsheet Model - Approach

The purpose of this work was to present the designer with a fast spreadsheet model that relates the microstructural information and chemistry to the yield strength as a function of temperature. The objective was to retain an accurate description of the mechanistic model at dislocation level and to include all variability of microstructure, and yet convert microstructural variables and chemistry to yield strength as a function of temperature at little computational expense. The approach is shown schematically in Figure 2.

The concept was to maintain all the physics of the model in a computationally expensive discrete dislocation dynamics simulations model, but extract its essence to derive a spreadsheet model. This extraction was done using a parametric study conducted using the numerical model. The results of this study were used for constructing analytical expressions through curve-fitting procedures. The parametric study included variable combinations that captured the effects of variable interactions. A heuristic model combined with the analytical expressions was derived to capture the interactions between the variables. This resulted in a model that predicts the room temperature critical resolved shear stress. To add the temperature effects, the variations of APB energy and friction stresses with temperature were used. Finally, a Taylor factor and Hall-Petch coefficients for the γ' and ($\gamma+\gamma'$) grains were used to predict yield strength of polycrystals. For all of these, data available in the literature were used to the extent possible. Thus in the final model, the only "fit" parameter turned out to be the APB energy. Even the values for

APB energy is known within reasonable bounds, and the values needed to fit data were well within these bounds. Finally, the APB energy was not allowed to vary within a given composition of the alloy. Thus all heat-treatments effects are actually predicted, with no fit parameters, while the chemical effect was predicted using only one parameter, the room temperature APB energy.

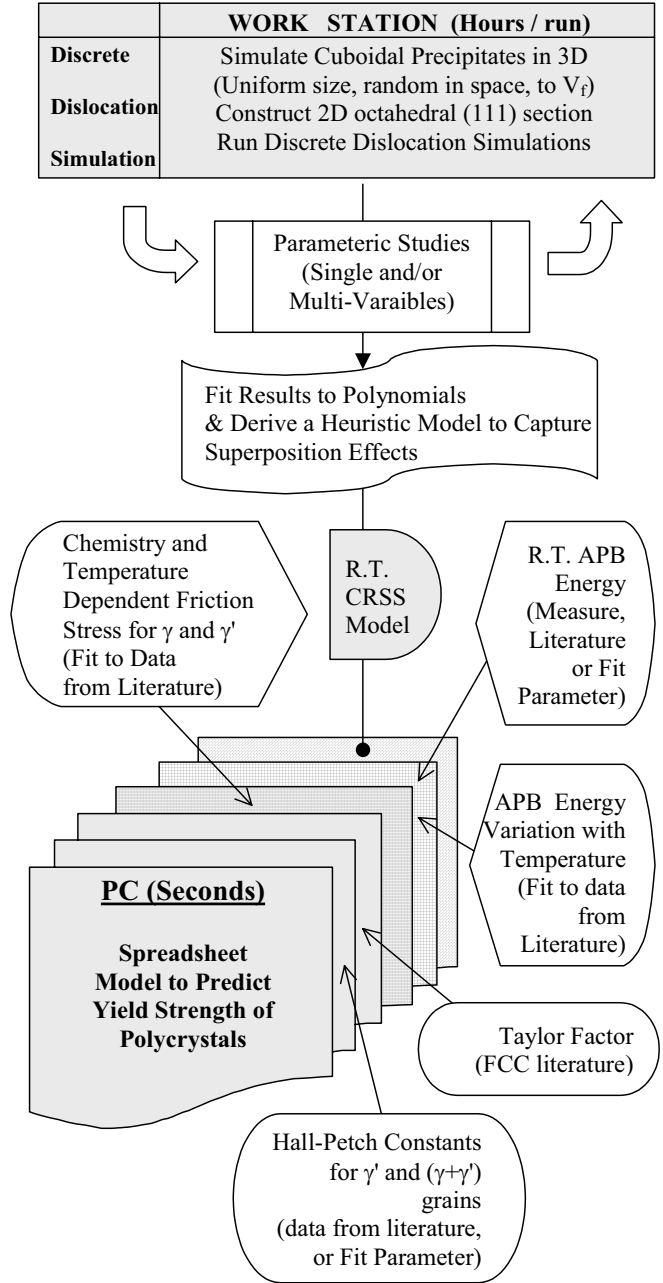


Figure 2: A schematic flow chart describing the approach that was used to extract the essence of the computationally intensive numerical DD model and add relevant features to obtain a fast spreadsheet model for predicting the yield strength of polycrystal superalloys.

4.0 Derivation of the Model

The steps shown in Figure 2 are detailed below in the sequence they appear in the figure.

4.1 Discrete Dislocation Simulation

The discrete dislocation model involves two steps, (1) generation of a 3-dimensional simulated microstructure and (2) simulation of a dislocation percolation through a 2-dimensional microstructure obtained by taking an octahedral (111) section of the simulated microstructure. The critical resolved shear stress is taken to be the minimum stress at which a pair of dislocations can pass through an entire microstructure. The dislocation percolation model is based on the well-established metallurgical principles of dislocation motion. The dislocations are assumed to pre-exist and their motion is modeled accurately using the method of Newton's laws of kinetic motion. The model is detailed elsewhere⁷ and only the relevant details are given here.

4.1.1 Microstructure Generation

The glide system in both γ and γ' is $\langle 110 \rangle \{111\}$ so a natural set of Cartesian axes is $x = \langle 110 \rangle$, $y = \langle 112 \rangle$, $z = \langle 111 \rangle$. The precipitates were assumed to be cuboidal in shape with a uniform size, 'a'. The 3-dimensional distribution is constructed by filling a rectangular parallelepiped with cubes of side 'a', using a random number generator for spatial location of each precipitate. The cubes are oriented the same as the crystallographic unit cells for γ and γ' , i.e., their body diagonals are parallel to z (Fig.3). Overlaps between precipitates were forbidden and precipitates

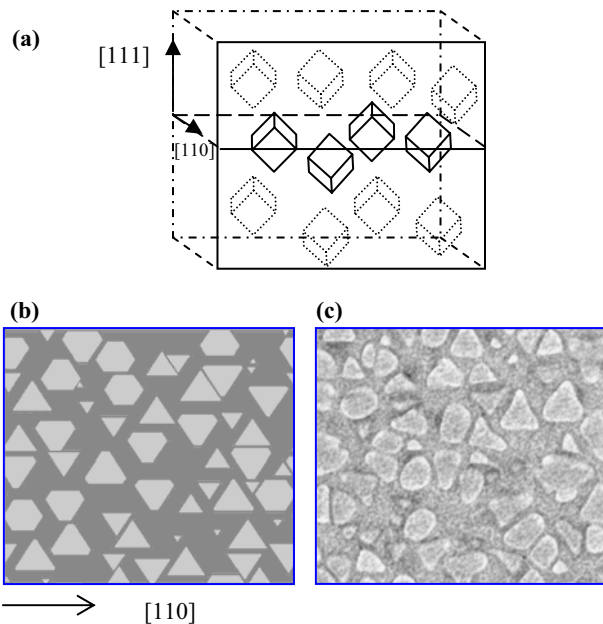


Figure 3: Computer Simulation of the microstructure of a Ni-based superalloy. (a) Cubes are placed at random locations in a parallelepiped to fill space up to a predetermined volume fraction of 0.4 (b) The intersections of the cubes on a (111) section show triangles and irregular hexagons. (c) A representative microstructure (courtesy: M. Uchic, AFRL/MLLM) of the (111) section of a Ni-based superalloy grain showing triangles and irregular hexagons of γ' dispersed in γ . Comparison of (b) and (c) testify to the simulation procedure.

were placed in the parallelepiped until the total volume fraction of precipitate reached a predetermined value. After generating the 3-dimensional microstructure of a given volume fraction, an octahedral section is taken (perpendicular to z). The intersections of this plane with the cubes are used to form a 2D image. The resultant image was a plane with a random array of equilateral triangles and irregular hexagons of varying sizes, the variations in size arising purely from randomness of the locations of the cubes. Figure 3 schematically shows the simulation procedure, along with an experimental (111) section of a $(\gamma+\gamma')$ grain of an industrial superalloy disk of IN100.

4.1.2 Discrete Dislocation Percolation

The glide system in both γ and γ' is $\langle 110 \rangle \{111\}$. Since the precipitates are coherent with the matrix, a matrix dislocation can enter and cut the precipitate; however an APB is created which offers a resistance to the cutting. Alternately the dislocation can bypass by bowing between the precipitates. The objective of the simulation is to obtain the critical stress required to percolate a dislocation pair through the 2-D array of precipitates, either by cutting, bowing or a combination of the two. The literature on TEM images of dislocations overwhelmingly favor the dislocation pair mechanism, where the first dislocation ($1/2\langle 110 \rangle$ in the matrix) upon entering the precipitate creates a plane of APB which is annihilated by the entrance of the second ($1/2\langle 110 \rangle$) dislocation behind it. Within the precipitate the two dislocations are connected through the APB and thus the pair is a superdislocation while in γ' .

At the start of a simulation of glide, a pair of $a/2\langle 110 \rangle$ dislocations (i.e., a superdislocation when in γ') is placed along one edge of the glide plane, parallel to x (a $\langle 110 \rangle$ direction). The dislocations are either screw or mixed (60°) in character. Since the self-stress, rather than the line tension approximation, is used, each dislocation is formed from a large number (about 400) of straight segments, joined at nodes. At each iteration of the simulation, the force acting at every node is calculated, the node is stepped by some small distance related to the force, and the new shape of the dislocation is thereby determined. When the forces on all segments come to zero, the dislocation stops. An example of the final state of a dislocation pair subjected to a stress below the critical value for complete percolation is shown in Figure 4. Note that the first dislocation has entered the precipitates at several locations but stopped by the APB that forms behind it. At the same time, the dislocation bows between precipitates, often enhancing the probability of entering the precipitate since it is easier to enter from the corner than from the edge.

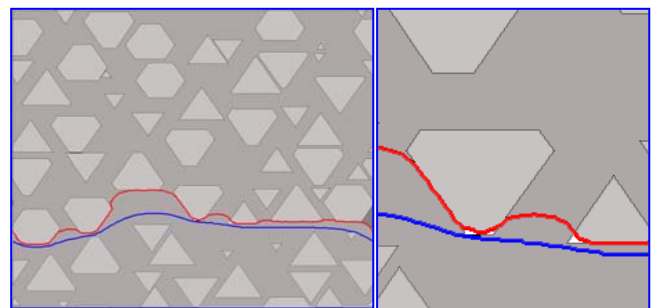


Figure 4: The final state of a dislocation pair subjected to a shear stress that is less than the critical stress for complete percolation. The higher magnification shows how the first dislocation stops after entering the precipitate.

This last point about bowing-assisted cutting is important. Clearly a planar interface will be cut only when the stress exceeds the value (Γ/b) for a single dislocation and $0.5(\Gamma/b)$ for a pair. This has been verified in the current simulation. However when the interface is discontinuous with provisions for bowing between such discontinuities being allowed, the critical stress is much lower, often around $0.25(\Gamma/b)$. Thus the actual distribution of the interfaces is an important feature to be captured in a model to calculate the true critical resolved shear stress.

The finer details of the simulation are detailed elsewhere.⁷ It is sufficient to mention here that the force at each node was calculated accurately and the computation included the following; (1) the long-range forces between dislocation segments and between the two dislocations of the pair, (2) the short-range forces that arise from local curvature effects, (3) the APB drag force, (4) coherency strain from lattice mismatch between the matrix and precipitate and (5) applied stress. The forces are summed algebraically at each node and the nodes are moved as though they are particles with effective masses and damping constants. The process is repeated iteratively until all dislocation segments come to a halt or move through the entire microstructure.

The smallest applied stress at which the dislocation pair percolates completely through the precipitate array is taken to be the critical resolved shear stress of the material. Repeating the entire simulation with differently positioned, but otherwise identical precipitates, gives a measure of the statistical scatter in the calculated yield stress arising from sampling (sectioning) error. For each simulation 5 different random seeds were studied. The standard deviation on the critical stress was nearly 10 MPa for a CRSS of 280 MPa.

4.2 Parametric Studies

The model uses several microstructural parameters as inputs. These are listed below.

- 1) APB Energy
- 2) Size of γ'
- 3) Volume Fraction of γ'
- 4) Coherency Strain
- 5) Mixed or Screw Dislocation
- 6) Matrix Friction Stress
- 7) Precipitate Friction Stress

Of the above, the size and volume fraction of the precipitates are usually available in the form of mean values. Distributions are not available. The coherency strain is reported in the literature to be near 0.15% from room temperature up to 1500°F in superalloys.⁸ The mixed dislocation was always found to be more resistant to motion and hence used for all the results presented in this work. The friction stresses in the matrix and precipitate are generally unknown, although a formalism is shown and used in the spreadsheet model (section 4.4).

The parameters listed above were varied one at a time, and the effect on the percolation stress calculated. The results are shown in Figures 3 and 4. The lines in these plots are the curves as given by the analytical expressions that were obtained by curve fitting to the simulation results. The error bars refer to one standard deviation of the scatter obtained from different seeds for the random number generator of the simulation code.

The results show that among the various parameters studied, the CRSS is most influenced by the APB energy, volume fraction, and matrix friction stress. The dependencies on APB energy and precipitate size are different from analytical models, e.g., Reppich et al.⁶ The volume fraction effect is as expected from analytical models. The effects of matrix and precipitate friction stresses are shown to be vastly different and the analytical models do not address this.

Finally the effect of a combination of secondary and tertiary precipitates was examined. The same simulation method was used and cubes of different sizes were randomly placed and a (111) section taken. The effect of the combination, of such a bimodal distribution, followed very nearly the rule of mixtures.

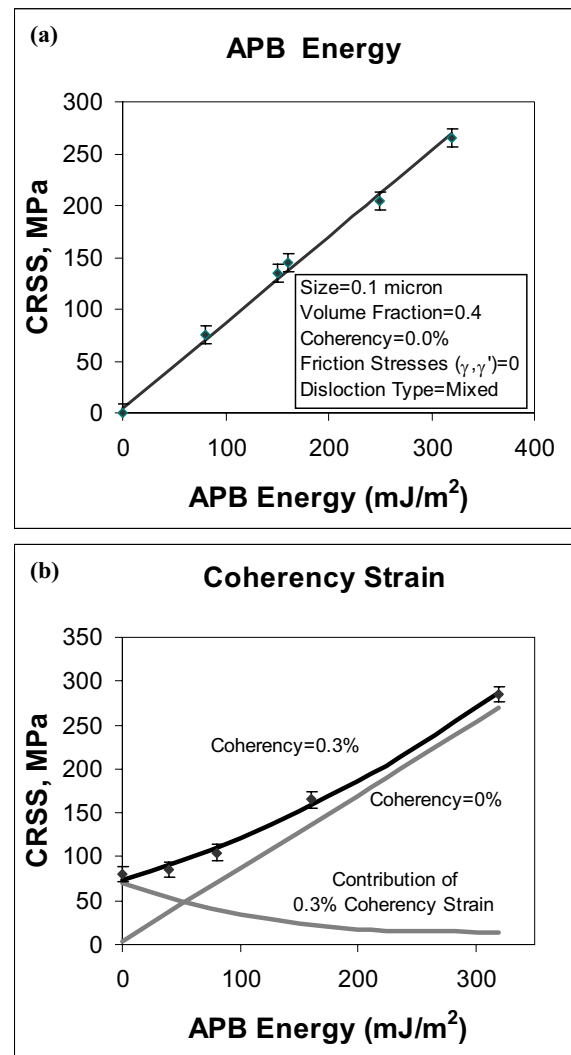


Figure 3: Results of a parametric study conducted using the discrete dislocation model showing the effects of APB energy and coherency strain. Note that the two effects interact. The effect of coherency strain on the CRSS depends on the APB energy. The solid lines are curve-fits using expressions given in section 4.3.

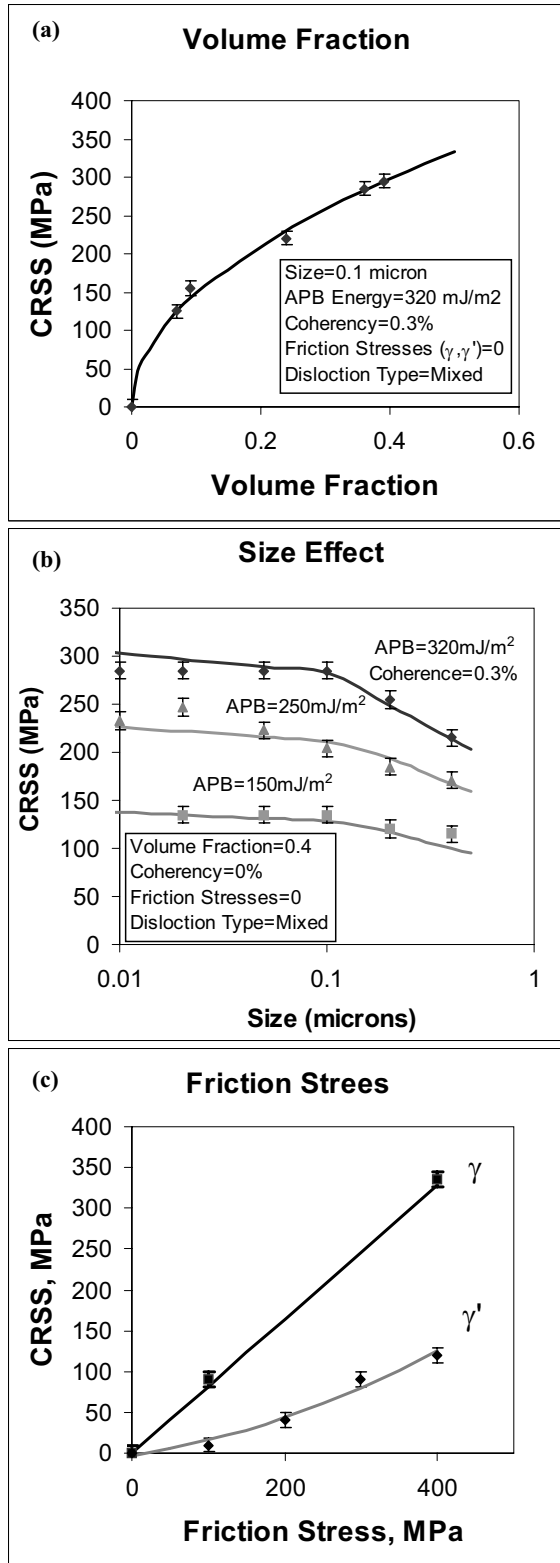


Figure 4: Results of a parametric study conducted using the discrete dislocation model showing the effects of precipitate volume fraction, precipitate size and friction stresses. The solid lines are the curve-fits using the analytical expressions given in section 4.3

4.3 CRSS Model from Polynomial Fits

From the above parametric studies, a set of expressions was derived through curve-fitting procedures, for the effect of each variable. The functional forms with best fits are given below.

APB Energy, Γ_{APB}

$$a_1 + a_2 \Gamma_{APB} \dots (1)$$

Coherency Strain, ϵ_{COH}

$$(c_1 + c_2 \Gamma_{APB} - c_3 \Gamma_{APB}^2 - c_4 \Gamma_{APB}^3) \frac{\epsilon_{COH}}{0.003} \dots (2)$$

Volume Fraction, V_f

$$(qV_f)^{0.5} \dots (3)$$

Precipitate Size, a

$$S_1 [a(V_f^{-0.5} - 1)]^{-S_2} \dots (4)$$

Matrix and Precipitate Friction Stresses, τ_γ & $\tau_{\gamma'}$

$$F \left\{ \left[P_1 + P_2 \tau_{\gamma'} + P_3 \tau_{\gamma'}^2 \right], \left[n_1 \tau_{\gamma'}^{n_2} \right] \right\} \dots (5)$$

The expressions were then linked heuristically in such a way as to be consistent with the results of the numerical simulations. The resulting model corresponded with the values shown in Fig.3 and 4 within 5%. The CRSS thus computed is then used to calculate the yield strength, σ_y , of a polycrystal using the Taylor factor, M and Hall-Petch coefficients, k, for the ($\gamma+\gamma'$) grains and the γ' grains.

$$CRSS = f(\text{expressions 1, 2, 3, 4, 5}) \dots (6)$$

$$\sigma_\gamma = (1 - f_{\gamma'}) \left\{ (M (CRSS) + k_{\gamma+\gamma'} d_{\gamma+\gamma'}^{-0.5}) \right\} + f_{\gamma'} (\tau_{\gamma'} + k_{\gamma'} d_{\gamma'}^{-0.5}) \dots (7)$$

In equation 7, f, k and d refer to volume fraction, Hall-Petch constant and grain size respectively, with the subscripts referring to the type of grain.

4.4 Matrix and Precipitate Friction Stresses

The ideas for expressing the effect of chemistry on the friction stresses were borrowed from Roth et al.⁹ and Kozar et al.¹⁰ The work of Roth has consolidated the literature data available on the solution strengthening effect in nickel along with a semi-empirical model that describes the effects through a list of

parameters. These parameters were used directly. To obtain the effect of temperature, the data summarized by Roth et al. and those of Clement et al.^{11,12} and Nitz et al.¹³ were used to derive a semi-empirical relation between chemistry, temperature and friction stress. The form used for the friction stress is given by the following equation (ref. Kozar et al.¹⁰, Roth et al.⁹).

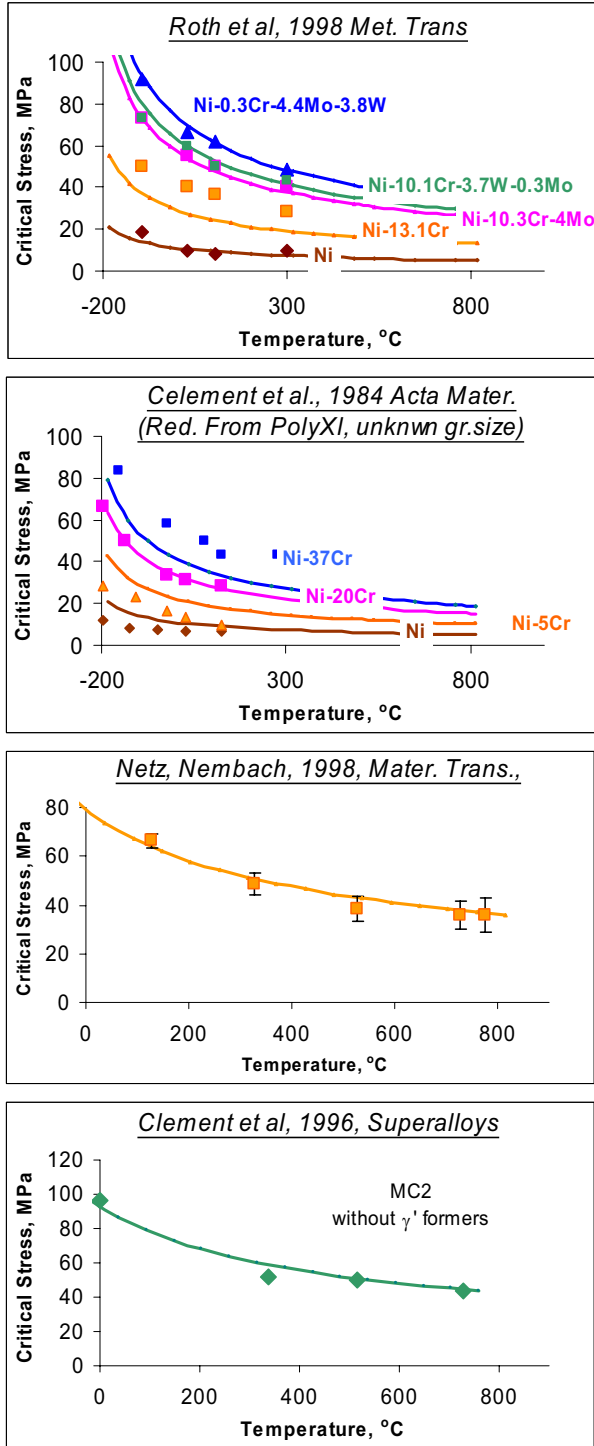


Figure 5 : The model for the friction stress of γ as a function of chemistry and temperature as given by equation 8 is shown compared with data from the literature.(Ref. 9-13)

$$\tau(\gamma) = \tau_o(\gamma) + (k1/T)^{k2} \left[\sum_{allsolutes} (\delta\tau / \partial C_{solute,\gamma}^{0.5}) C_{solute,\gamma}^{0.5} \right] \dots \quad (8)$$

Here $\tau_o(\gamma)$ is the friction stress of pure Ni, $C_{solute,\gamma}$ refers to the concentration of solute in the matrix, γ . The fit of the equation 8 to the data in the literature is shown in Figure 5. The effect of solute and temperature on the friction stress of γ' was modeled as follows (ref. Kozar et al.¹⁰).

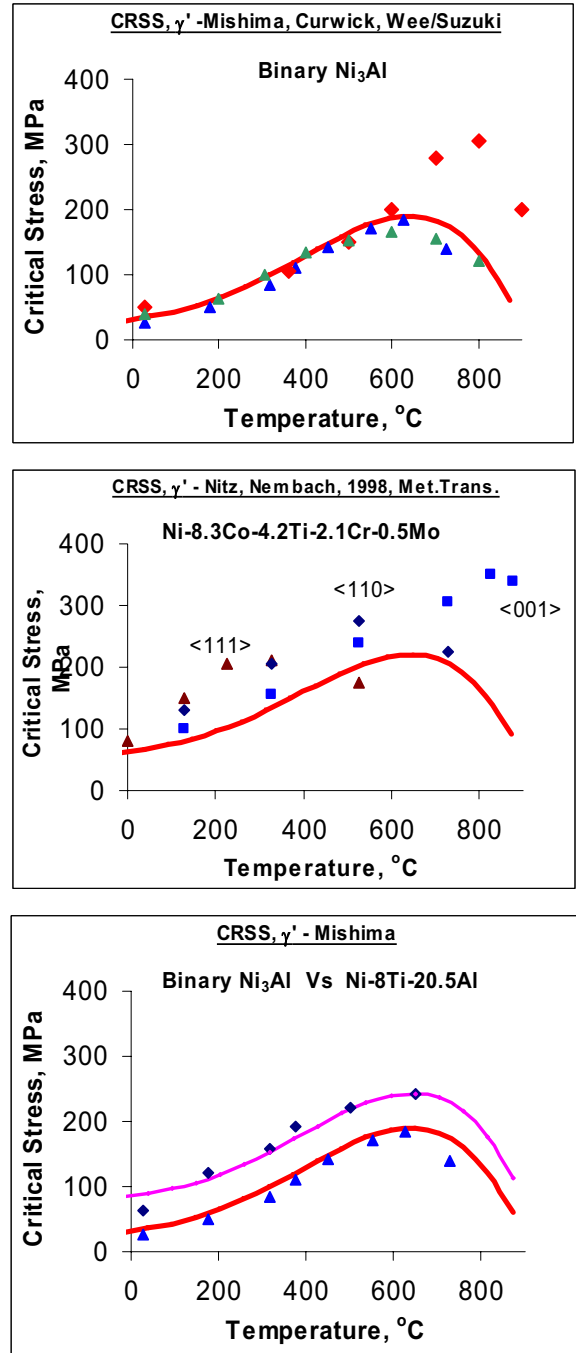


Figure 6 : The fit of Equation 9 (Ref.10) to the friction stress data available in the literature (Ref. 14-18) for γ' alloys are shown compared.

$$\tau(\gamma') = \tau_o(\gamma') + \left[\sum_{\text{allsolutes}} (\delta\tau / \partial C_{\text{solute},\gamma'}) C_{\text{solute},\gamma'} \right] + \dots(9)$$

$$+ [q_1 T + q_2 T^2 + q_3 T^3 + q_4 T^4]$$

Here $\tau_o(\gamma')$ is the friction stress of binary Ni₃Al, $C_{\text{solute},\gamma'}$ refers to the concentration of solute in the matrix, γ' . The parameters were same as in ref.10. Again, the fit of equation (9) to the data in literature is shown in Figure 6.¹⁴⁻¹⁸ Note that the orientation dependence (Schmid factor violation) is not included in the model.

4.5 Temperature Dependence of APB Energy

The APB energy of the γ' phase is one of the key parameters of the model as seen from Figure 3. Unfortunately it is also among the least well known parameters. However, the value of the APB energy can be bounded from data available in the literature to be between 150 and 350 mJ/m².¹⁹⁻²¹ Further, APB energy is also known to be a function of chemistry.^{20,22,23} The actual value and the chemical dependence are beyond the scope of this work and they may remain uncertain for several more years to come. Meanwhile, the APB energy shall remain a fit parameter, although it is restricted to be within the range mentioned above.

Independent of the above uncertainty, it appears that a reasonable estimate of its temperature dependence can be inferred from two sources of literature work.^{24,25} One of them is experimental²⁵ while the other is theoretical.²⁴ Due to the importance of this variation, we have attempted to derive a temperature dependence for APB energy based on this literature information. The formalism that best fits the information is as follows.

$$\Gamma(T) = (\Gamma_o) \exp(-T/T^*) \dots (10)$$

The literature data is shown compared with Eqn 10 in Figure 7.

4.6 Hall-Petch Coefficients and Taylor Factor

The Hall-Petch coefficients for the $(\gamma+\gamma')$ grains and the

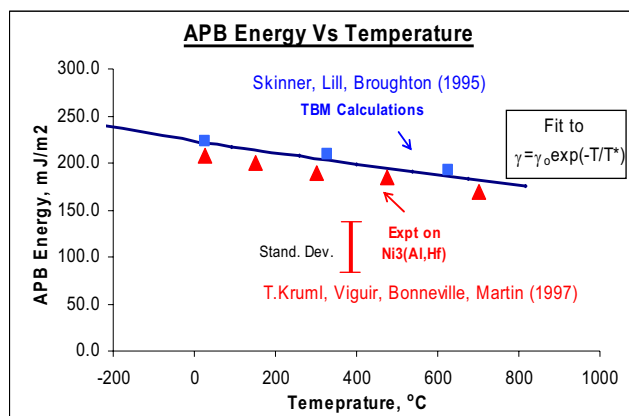


Figure 7 : The variation of APB energy with temperature is modeled using a simple exponential law that was fit to data in the literature (Ref.24, 25)

primary γ' grains are unknown. Although several values have been reported for superalloys, there is no systematic study in which the grain size was independently varied. The values for polycrystalline γ' show large variability from 500 to 2000 MPa- $\mu\text{m}^{1/2}$, while nickel and other fcc metals typically have coefficients of the order of 200 MPa $\mu\text{m}^{1/2}$.²⁰ The issue is further complicated by the fact that the superalloys of interest here contain a mixture of two different types of grains. Clearly, it makes sense to assume that both γ and $(\gamma+\gamma')$ grains share a single value. Thus in this work, there was only one parameter that was used and it was considered as a fit parameter, but well within the known bounds. The Taylor factor was taken to be 3, which is a fairly well established value for polycrystalline fcc metals and alloys.^{26,27}

5.0 Predictions of the Spreadsheet Model

The model was written as a spreadsheet using Microsoft Excel. The input parameters are specified in a single worksheet, while the other worksheets are used to compute the various parameters and predict the yield strength as a function of temperature. The input parameters included composition of the two phases in addition to the microstructural parameters. For all the alloys the Hall-Petch constants for both the $(\gamma+\gamma')$ grains and primary γ' grains were held constant at 450 MPa- $\mu\text{m}^{1/2}$ and the coherency strain was taken to be 0.1%. The APB energy was the only fit parameter.

5.1 Nimonic 105

The data of Nitz and Nembach¹³ is of particular value since they had measured the friction stresses of the γ , and γ' separately and measured the CRSS of single crystal of superalloy composition (Nimonic 105) with a microstructure consisting of γ

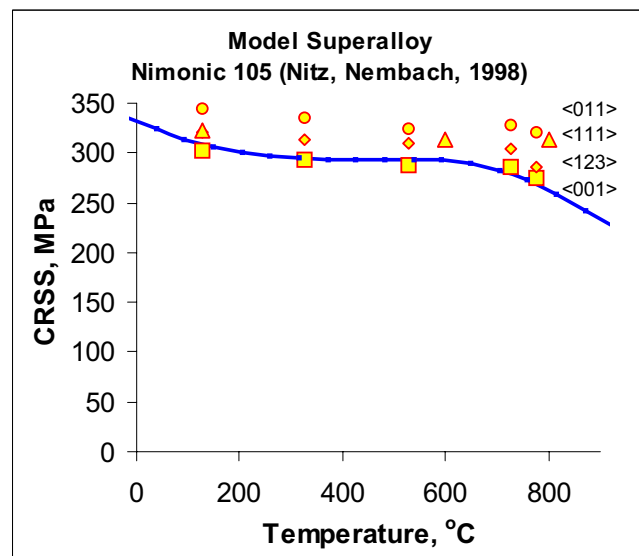


Figure 8 : A comparison of the predictions, of the CRSS of single crystal of composition that of Nimonic 105, compared with the experimental data at different orientations (Ref.13) The only fit parameter was the APB energy (260 mJ/m²) which is well in the range expected. A value of 260(+20,-40) mJ/m² has been reported in a recent work (Ref.21) for the APB energy. Note that the orientation effect (Schmid factor violation) in friction stress of γ' is not included in the model.

and γ' of the same compositions. They had measured all of these as a function of temperature. This data set is thus an ideal set to validate the model. A comparison of the model with the data is presented in Figure 8. Note that the model does not capture the orientation dependence, since the orientation dependence of the friction stress of γ' is not included in model.

The only fit parameter, as mentioned earlier, is the APB energy (Γ_o) and the predictions are for a value of 260 mJ/m^2 . In a more recent work co-authored by Nembach²¹, an APB energy of $260(+20, -40) \text{ mJ/m}^2$ has been reported for the γ' in Nimonic 105. The model is found to predict results for this alloy reasonably well.

5.2 Binary Model Superalloy (Ni-15Al)

A binary alloy of Nickel and Aluminum, Ni-15Al, has been reported on in the literature.²⁸ This is of interest since the system has no alloying elements. The γ' was taken to be of composition Ni-25Al. The literature has both microstructural and mechanical property data for this alloy. The model predictions are compared in Figure 9. With a reasonable choice of APB energy (195 mJ/m^2), the data and model agree quite well. APB energies of 160 to 220 mJ/m^2 have been reported for unalloyed Ni_3Al in the literature.^{19,20,22,23}

5.3 Superalloy ME3

Another class of superalloys for which both microstructural values and mechanical property data are available in the literature is the newer class of disk alloys, termed ME3.²⁹ Compositions of the individual phases were not available; they were estimated using partitioning ratios. The data and model predictions are shown compared for two different heat-treated conditions in Figure 10. The APB energy needed for the fit was 320 mJ/m^2 , higher than that for Nimonic 105 alloys. The reason for the higher value of APB energy is not clear; note that the model uses APB energy as the only fit parameter; using higher

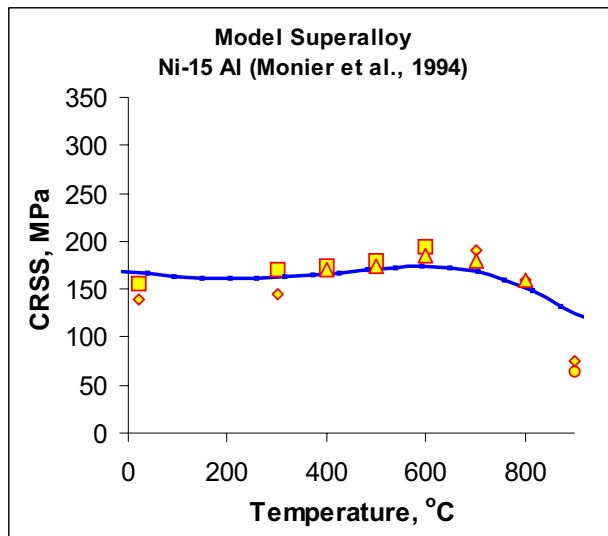


Figure 9 : The data and model predictions are shown compared for a binary Ni-15Al model single crystal alloy.(Ref.30) The Hall-Petch constant was held the same at $450 \text{ MPa}\mu\text{m}^{0.5}$ and the APB energy of 195 mJ/m^2 which is consistent with literature data (Ref. 19, 20, 22, 23)

matrix friction stress might have given an equivalent fit. From Fig.10, it is seen that the model captures the heat treatment effects well.

5.4 IN100 and René88 Alloys

Data on current industrial superalloys IN100 and René88 were obtained from the manufacturers, Pratt & Whitney and General Electric respectively. Both mechanical test data and microstructural information, including phase compositions were made available.

For the IN100 alloys, several alloys with varying heat treatments and compositional modifications were made available (Courtesy : J.Schirra, P&W). A value of $260\pm 60 \text{ mJ/m}^2$ was measured by Dimiduk on IN100 superalloy.³⁰ For a single choice of APB energy of 260 mJ/m^2 for all the alloys, the predictions are shown compared with the data in Figure 11; the correspondence is seen to be reasonable. Predictions for some alloys, which were

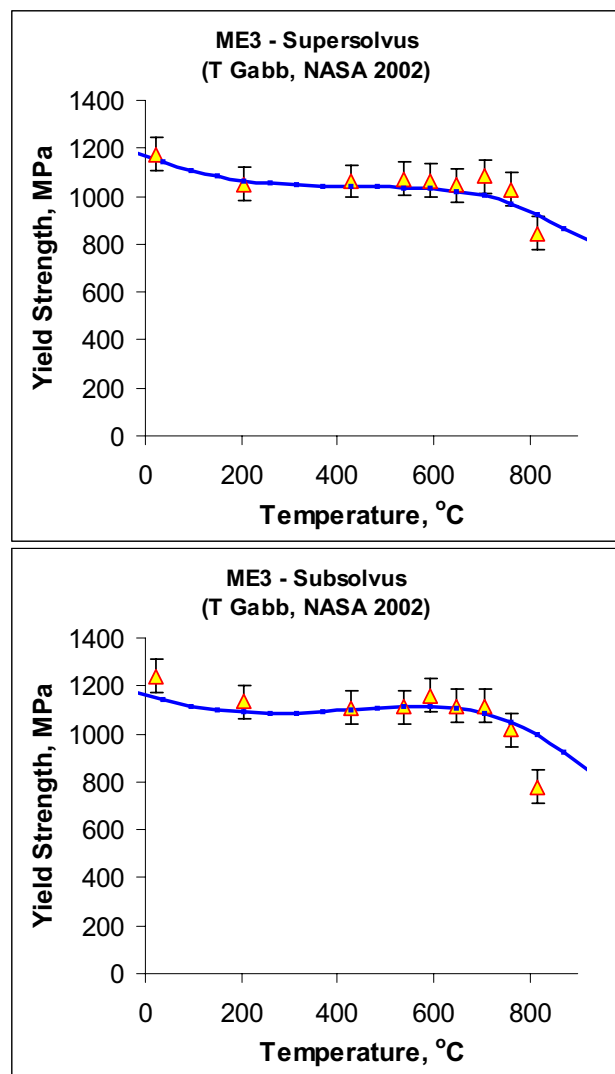


Figure 10 : The data and model predictions are shown compared for a high temperature disk alloy, ME3 (Ref.29). The Hall-Petch constant was held the same at $450 \text{ MPa}\mu\text{m}^{0.5}$ and the APB energy required for the fir was 320 mJ/m^2 . The predictions for the effect of heat treatment is seen to be reasonable.

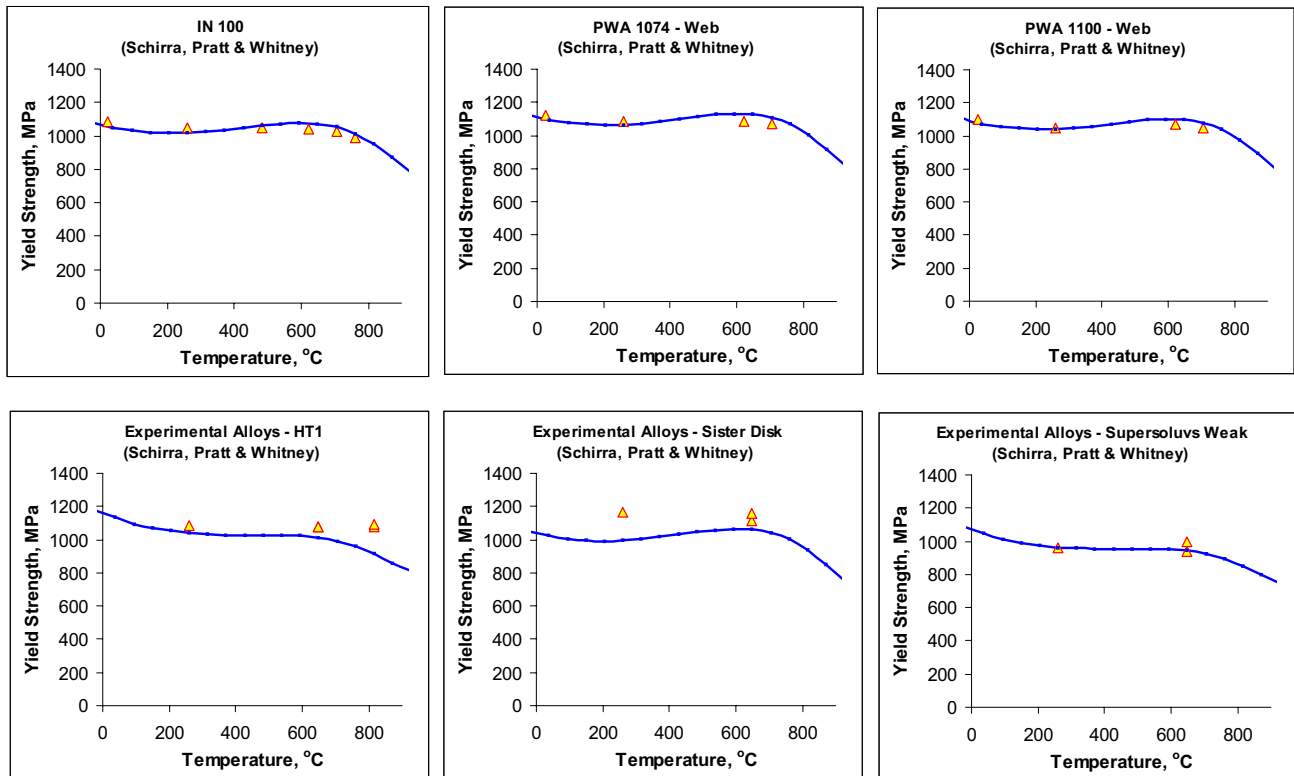


Figure 11 : Data on IN100 and a series of alloys of varying heat treatments and compositions (based on IN100) are shown compared with the model predictions. The predictions are based on microstructural information provided by Pratt & Whitney (Courtesy; J.Schirra). The APB energy for the fit was 260 mJ/m², while the experimental value measured on IN100 was 260 ± 50 mJ/m² (Ref.30).

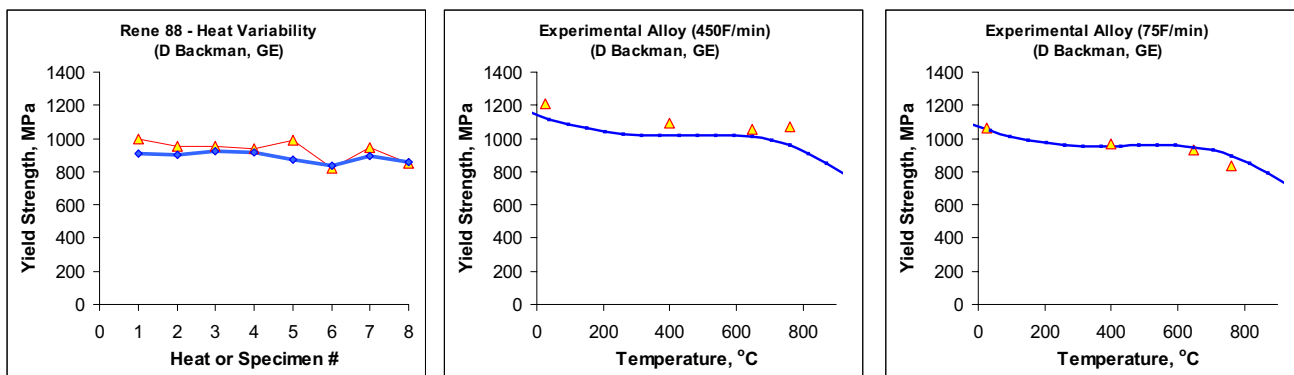


Figure 12 : Data on the variability between heats in a René88 alloy and data on two alloys nominally of René88 composition but with varying heat treatments, are shown compared with the model predictions. The predictions were based on microstructural information provided by GE (Courtesy; D Backman). The APB energy for the fit was 260 mJ/m².

prepared as experimental alloys and which deviated significantly from the industrial standard in both microstructure and properties, were found to be predicted with less accuracy. It is believed that precipitate morphology could explain these differences.

For the René88 alloys, heat-to-heat variability in microstructures and corresponding yield data were made available (courtesy : D.Backman, GE). In addition data on two experimental alloys with compositions nominally the same as René88 but with

very different heat treatments (cooling rates) were made available. Again, good correspondence was obtained for all these alloys, with a value of 260 mJ/m² for the APB energy (see Figure 12).

6.0 Limitations of this Work

While the spreadsheet model is fast and predicts yield strength for a variety of superalloys reasonably well, it is worth taking stock of the assumptions and limitations of this work.

The first limitation of this work is the assumption of cuboidal shape for the precipitates. More recent work with the discrete dislocation model has shown variations of up to 10% with the shape of the precipitates from cubes to spheres. Second, although the 2D section provided a range of sizes for the dislocation percolation simulation, the precipitate simulation procedure used cubes of a uniform size. The effect of distributions in size in 3D will likely be the focus of future work. Third, the current model was not designed to predict the effect of different orientations of single crystals. Finally, the spreadsheet model was fit to a limited range of parameters investigated; validity of the model beyond this range is unknown. Better models might be possible than the one generated and used here; no optimization was attempted. These are limitations as far as prediction of the CRSS is concerned.

In extending the CRSS values to polycrystalline yield strength and in predicting temperature dependences, further assumptions and limitations are to be pointed out. The distribution in size of grains was ignored and a simple Taylor factor was used to account for the polycrystal. Clearly more detailed models that consider distributions in size and misorientations will be more accurate. Second, it is not clear if the anomalous increase in friction stress of bulk γ' alloys will be experienced by the dislocations in the small (0.1 micron) γ' precipitates. Third the variation of APB energy with temperature is not well known and the information in the literature is scant. Fourth, the variation of precipitate size and/or volume fraction with temperature was neglected. Finally, the effect of chemistry on the APB energy will be an important factor that will need to be determined experimentally or through first principles calculations to much higher level of precision than is available today.

7.0 Summary

A model that retains the physics and/or mechanistic principles but enables fast calculations of the yield strength of superalloys was developed. A fast spreadsheet model has been derived for possible use in design with alloys. The model uses microstructural parameters as input and predicts the yield strength as a function of temperature. The predictions are reasonable for a wide range of superalloys and shows considerable promise.

8.0 Acknowledgments

We are pleased to acknowledge several useful discussions with Mr. J. J. Schirra of Pratt & Whitney, Dr. D. Backman of GE(CRD), and Prof. T. M. Pollock (U.Mich.), from whom we derived useful insights. The data on IN100 and René88 alloys kindly provided by J.Schirra (PW) and D. Backman (GE) are acknowledged. We thank Prof. T. M. Pollock for sharing work before publication. We would also like to thank Dr.L.Christodoulou of DARPA and Dr.R.E.Dutton of AFRL for support and encouragement throughout the work.

9.0 References

1. J.J. Schirra, and S.H. Goetschius, Development of an Analytical Model Predicting Microstructure and Properties Resulting from the Thermal Processing of a Wrought Powder Nickel-Base Superalloy Component, S. D. Antolovich *et al.*, Eds., Superalloys 1992 (TMS, 1992).

2. J. Friedel. Les Dislocations, Gauthier-Villars, Paris, 1956.
3. E. Nembach. Particle Strengthening of Metals and Alloys, Wiley & Sons, New York, 1996.
4. B. Reppich, in *Materials Science and Technology* R. W. Cahn, H. P, E. J. Kramer, Eds. (VCH Verlagsgesellschaft mbH, Weinheim, 1993), vol. 6, pp. 311.
5. A.J. Ardell, in *Intermetallic Compounds* J. H. Westbrook, R. L. Fleischer, Eds. (Wiley & Sons Ltd., New York, 1994), vol. 2, pp. 257-286.
6. B. Reppich, *Acta Metall.*, **30** 87-94 (1982).
7. S.I. Rao, T.A. Parthasarathy, D.M. Dimiduk, and P.M. Hazzledine, *Phil. Mag.*, (submitted).
8. H. Biermann, M. Strehler, and H. Mughrabi, *Metallurgical and Materials Transactions*, **27A** [4] 1003-1014 (1996).
9. H.A. Roth, C.L. Davis, and R.C. Thomson, *Metallurgical and materials transactions A*, **28A** [6] 1329-1335 (1997).
10. R. Kozar, J. Schirra, W. Milligan, and T.M. Pollock, *Mater. Trans.*, (submitted).
11. N. Clement, D. Caillard, and J.L. Martin, *Acta Metall.*, **32** [6] 961-975 (1984).
12. N. Clement, A. Coujou, M. Jouiad, P. Caron, H.O.K. Kirchner, and T. Khan. Local Order and Mechanical Properties of the g Matrix of Nickel-Base Superalloys, in Superalloys 1996, pp239-248, (1996)
13. A. Nitz, and E. Nembach, *Metallurgical and Materials Transactions*, **29A** [3] 799-807 (1998).
14. T. Suzuki, Y. Oya, and D.M. Wee, *Acta Metall.*, **28** 301 (1980).
15. L.R. Curwick, Doctoral Dissertation, University of Minnesota (1972).
16. Y. Mishima, S. Ochial, and Y.M. Yodogawas, *Trans. JIM*, **27** 41 (1986).
17. P.H. Thornton, and R.G. Davies, *Metallurgical Transactions*, **1A** 549 (1970).
18. O. Noguchi, Y. Oya, and T. Suzuki, *Metall. Trans.*, **12A** 1647 (1981).
19. T. Kruml, E. Conforto, B.L. Piccolo, D. Caillard, and J.L. Martin, *Acta Mater*, **50** 5091-5101 (2002).
20. M. Yamaguchi, and Y. Umakoshi, *Progress in Mater. Sci.*, **34** 1-148 (1990).
21. D. Baither, C. Rentenberger, H.P. Karnthaler, and E. Nembach, *Phil. Mag.*, **82** [9] 1795-1805 (2002).
22. D.M. Dimiduk, *J de Phys.*, **III** [1] 1025 (1991).
23. D.M. Dimiduk, A.W. Thompson, and J.C. Williams, *Phil. Mag. A*, **67** 675-698 (1992).
24. A.J. Skinner, J.V. Lill, and J.Q. Broughton, *Modell. Simul. Mater. Sci. Eng.*, **3** 359-369 (1995).
25. T. Kruml, B. Viguier, J. Bonneville, and J.L. Martin, *Mater. Sci. & Eng.*, **A234-236** 755-757 (1997).
26. U.F. Kocks, *Metall. Trans. A*, **1** 1121 (1970).
27. H. Mecking, U.F. Kocks, and C. Hartig, *Scripta Mater.*, **35** [4] 465-471 (1996).
28. C. Monier, C. Bertrand, J.-P. Dallas, M.-F. Trichet, M. Cornet, and P. Veysiere, *Mater. Sci. & Eng.*, **A188** 133-139 (1994).
29. T.P. Gabb, J. Telesman, P.T. Kantzos, and O.C. K, "Characterization of the Temperature Capabilities of Advanced Disk Alloy ME3", Tech. Report NASA/TM-2002-211796 (2002).
30. D.M. Dimiduk, *Unpublished Work*, (2003).